AIP | Journal of Applied Physics

Local electronic states of Fe4N films revealed by x-ray absorption spectroscopy and x-ray magnetic circular dichroism

Keita Ito, Kaoru Toko, Yukiharu Takeda, Yuji Saitoh, Tamio Oguchi, Takashi Suemasu, and Akio Kimura

Citation: Journal of Applied Physics **117**, 193906 (2015); doi: 10.1063/1.4921431
View online: http://dx.doi.org/10.1063/1.4921431
View Table of Contents: http://scitation.aip.org/content/aip/journal/jap/117/19?ver=pdfcov
Published by the AIP Publishing

Local electronic states of Fe_4N films revealed by x-ray absorption spectroscopy and x-ray magnetic circular dichroism

Keita Ito,[1,2,3,a)] Kaoru Toko,[1] Yukiharu Takeda,[4] Yuji Saitoh,[4] Tamio Oguchi,[5] Takashi Suemasu,[1] and Akio Kimura[6]
[1]*Institute of Applied Physics, Graduate School of Pure and Applied Sciences, University of Tsukuba, Tsukuba, Ibaraki 305-8573, Japan*
[2]*Department of Electronic Engineering, Graduate School of Engineering, Tohoku University, Sendai 980-8579, Japan*
[3]*Japan Society for the Promotion of Science (JSPS), Chiyoda, Tokyo 102-0083, Japan*
[4]*Condensed Matter Science Division, Japan Atomic Energy Agency (JAEA), Sayo, Hyogo 679-5148, Japan*
[5]*The Institute of Scientific and Industrial Research (ISIR), Osaka University, Ibaraki, Osaka 567-0047, Japan*
[6]*Graduate School of Science, Hiroshima University, Higashi-Hiroshima, Hiroshima 739-8526, Japan*

(Received 6 April 2015; accepted 11 May 2015; published online 20 May 2015)

We performed x-ray absorption spectroscopy (XAS) and x-ray magnetic circular dichroism (XMCD) measurements at Fe $L_{2,3}$ and N K-edges for Fe_4N epitaxial films grown by molecular beam epitaxy. In order to clarify the element specific local electronic structure of Fe_4N, we compared experimentally obtained XAS and XMCD spectra with those simulated by a combination of a first-principles calculation and Fermi's golden rule. We revealed that the shoulders observed at Fe $L_{2,3}$-edges in the XAS and XMCD spectra were due to the electric dipole transition from the Fe $2p$ core-level to the hybridization state generated by σ^* anti-bonding between the orbitals of N $2p$ at the body-centered site and Fe $3d$ on the face-centered (II) sites. Thus, the observed shoulders were attributed to the local electronic structure of Fe atoms at II sites. As to the N K-edge, the line shape of the obtained spectra was explained by the dipole transition from the N $1s$ core-level to the hybridization state formed by π^* and σ^* anti-bondings between the Fe $3d$ and N $2p$ orbitals. This hybridization plays an important role in featuring the electronic structures and physical properties of Fe_4N. © *2015 AIP Publishing LLC*. [http://dx.doi.org/10.1063/1.4921431]

I. INTRODUCTION

Anti-perovskite type transition metal ferromagnetic nitrides such as Fe_4N and Mn_4N were subjected to extensive study in order to apply them to novel magnetic devices over the past decades.[1–5] Figure 1 shows the crystalline structure of anti-perovskite type nitrides. One N atom is located at the body center of face-centered cubic lattice composed of transition metals. Here, we define the corner and face-centered atomic sites as I and II sites, respectively. In anti-perovskite type transition metal ferromagnetic nitrides, II sites are further divided into IIA and IIB sites representing the inequivalent features of the electronic structure related to the band hybridization with the N atom. The Curie temperature of Fe_4N was reported to be 767 K,[1] which signifies that its ferromagnetism is thermodynamically stable. There are several reports on the epitaxial growth of Fe_4N films on MgO(001),[6,9,10] $SrTiO_3$ (STO)(001),[7,9,10] $LaAlO_3$(LAO)(001),[9,10] and Cu(001)[8] substrates. Kokado *et al.* calculated the spin-dependent electrical conductivity of Fe_4N by a combination of the first-principles, tight-binding calculation, and the Kubo formula.[11] It predicts that, while the spin-polarization of the density of states (P_D) at the Fermi level (E_F) of Fe_4N to be −0.6, the spin-polarization of electrical conductivity (P_σ) to be −1.0. Thereby, Fe_4N is regarded as a promising material for spintronics applications. Here, the incorporated N atoms are considered to play an important role in generating high-spin polarization. Such a large magnitude of the negative spin-polarization at E_F in Fe_4N is theoretically attributed to the band hybridization between the orbitals of Fe $4sp$ at II sites and N $2sp$.[11] This hybridization eventually leads to a dominant contribution of Fe $3d$ states around E_F because Fe $4sp$ states are pushed above Fe $3d$ states.[11] Point contact Andreev reflection experiment for the Fe_4N films on MgO(001) showed that the measured spin polarization $|P_\sigma|$ was larger for Fe_4N than for α-Fe.[12] Furthermore, spin-resolved photoemission spectroscopy study revealed the negative P_D near E_F for Fe_4N films on STO(001) substrate.[13] Recently, a negative anisotropic magnetoresistance (AMR) effect was reported for Fe_4N films.[14–16] To clarify the observed AMR, Kokado *et al.* performed a model calculation and exhibited relationship between the sign of AMR signals and dominant *s-d* scattering process in ferromagnetic materials.[17] Here, *s* and *d* represent general conductive and localized electrons, respectively. As mentioned above, the Fe $3d$ electrons are expected to mainly contribute to the electrical transport in Fe_4N.[11] Following this model calculation, the negative AMR effect in Fe_4N was explained by dominant *s-d* scattering process of $s_\downarrow \rightarrow d_\downarrow$, and attributed to both negative P_D and P_σ.[17] A lot of other physical phenomena reported for Fe_4N such as an inverse tunneling magnetoresistance effect,[18] an inverse current induced magnetization switching,[19] and a high-efficiency spin pumping[20] can track back to the negative spin-polarization at E_F. Making good use of negative spin-polarization in materials will further develop novel spintronics devices.

a)Electronic mail: keita.ito.729@gmail.com

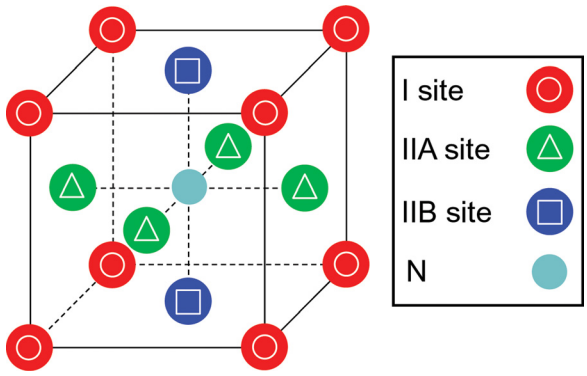

FIG. 1. Lattice structure of Fe_4N. II sites are distinguished by IIA and IIB sites due to the inequivalent features of the electronic structure related to the band hybridization with the N atom.

In order to unravel the underlying physics of such exotic magnetic properties, where the negative spin-polarization at E_F should play an important role, the site-resolved N 2*sp* and Fe 3*d* states need to be clarified. X-ray absorption spectroscopy (XAS) and x-ray magnetic circular dichroism (XMCD) are useful techniques that provide key information on the element specific electronic structures of the constituent elements in the material since core-level excitation energies can be tuned. Here, the Fermi's golden rule with electric dipole (E1) transitions allows us to determine the density of unoccupied electronic states in an element- and orbital-selective way. One can also clarify the element specific spin (m_{spin}) and orbital magnetic moments (m_{orb}) from the XMCD spectra using a well-known sum rule.[21,22] These XAS and XMCD techniques were applied to Fe_4N epitaxial films.[23–25] In our previous report, site-averaged m_{spin} and m_{orb} per Fe atom were evaluated to be 1.87 and 0.19 μ_B, respectively, and m_{orb}/m_{spin} value was 0.10 by XMCD measurements for Fe $L_{2,3}$-edges of Au/Fe_4N/LAO(001) at 300 K.[25] However, the site-specific electronic states of inequivalent Fe I and II sites as well as N sites are yet to be resolved. In this study, we compared the experimental XAS and XMCD spectra acquired at Fe $L_{2,3}$ and N *K*-edges of Fe_4N films with those calculated theoretically, and clarified the element specific local electronic structure in Fe_4N. To our knowledge, there have been no reports thus far on the theoretical calculation for XAS and XMCD spectra at Fe $L_{2,3}$-edge of Fe_4N. There is only one report on the line shapes of the XAS and XMCD spectra at N *K*-edge of Fe_4N calculated by the first-principles using FEFF code.[26] However, a comparison with experimental results is yet to seek.

II. EXPERIMENT

XAS and XMCD measurements were performed on Fe $L_{2,3}$ and N *K*-edges of epitaxially grown Au(3 nm)/Fe_4N (10 nm)/LAO(001) (sample A) and Fe_4N(20 nm)/STO(001) (sample B) by molecular beam epitaxy (MBE).[24] We confirmed epitaxial growth of Fe_4N layers in both samples A and B by reflection high-energy electron diffraction and out-of-plane x-ray diffraction. Though the substrates and layer thicknesses of Fe_4N were different between samples A and B, the Fe_4N films thicker than 10 nm are almost relaxed,[10] and thereby there is no difference in the degree of lattice strain between these two samples. After growth of the Fe_4N layer in sample A, a 3-nm-thick Au capping layer was subsequently deposited in the same MBE chamber. In contrast, we did not put the capping layer on sample B in order to minimize a loss of the weak XMCD signals of N *K*-edge. XAS and XMCD measurements by the total electron yield method were performed at the twin helical undulator beamline BL23SU of SPring-8 in Japan.[27] Circularly polarized soft x-rays were incident perpendicular to the film surface. External magnetic fields (H) of ± 3 T were applied perpendicular to the film surface during Fe $L_{2,3}$-edges measurements at 300 K. 3 T was enough to saturate the sample magnetization. XAS and XMCD spectra of N *K*-edge were measured at 100 K under $H = \pm 6$ T. We used averaged spectra for analysis to ensure the accuracy of the measurement.

III. CALCULATION

XAS and XMCD spectra at Fe $L_{2,3}$ and N *K*-edges of Fe_4N were simulated by a combination of the first-principles calculation using the all-electron full-potential linearized augmented-plane-wave method and Fermi's golden rule with E1 transitions. Self-consistent-field calculations were performed with the scalar relativistic scheme plus the spin-orbit coupling in the second variation at every iteration. Some more details of the methods were described in the previous paper.[28] The magnetization axis is assumed to be the Fe_4N[001] direction. Accordingly, the Fe IIA and IIB sites (see Fig. 1) become inequivalent in the E1 transitions.

IV. RESULTS AND DISCUSSION

Figures 2(a) and 2(b) show the experimental XAS and XMCD spectra, respectively, at Fe $L_{2,3}$-edges of the Fe_4N layer in sample A. We can clearly see the main peak structure at photon energies of 707.8 eV for Fe L_3- and 720.8 eV for Fe L_2-edges. The shoulders, denoted by arrows in Figs. 2(a) and 2(b), were observed at a photon energy of approximately 3 eV above the main peaks. Note that such shoulders observed in XAS and XMCD spectra of some metallic ferromagnetic systems have been successfully explained by unoccupied single-particle density of states.[29] One may anticipate that similar satellites and shoulders of the spectra appear due to the final state multiples caused by the local electrostatic coupling between a created core hole and *d* holes of the outer-shell. However, such final state multiplets are not likely in the present case because the photo-induced excited electrons cannot stay at the same atomic site due to the strong itinerancy of *d* electrons.

In order to clarify the origin of these line shapes, we obtained the density of states of Fe_4N by the first-principles calculation. Figure 3 shows the calculated spin- and orbital-resolved partial densities of states (p-DOSs) in Fe_4N. The left and right columns show the p-DOSs of majority and minority spins, respectively. The site-averaged m_{spin} and m_{orb} per Fe atom in Fe_4N are calculated to be 2.45 and 0.06 μ_B, respectively. These values are very close to those of reported calculation values.[5] However, the calculated m_{orb} of 0.06 μ_B is much smaller than the experimental m_{orb} of 0.19 μ_B, and

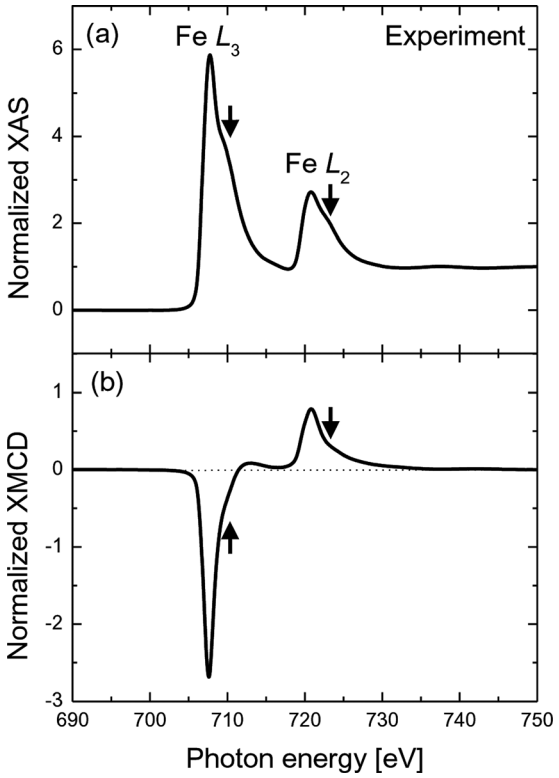

FIG. 2. Experimentally obtained (a) XAS and (b) XMCD spectra at Fe $L_{2,3}$-edges of the Fe_4N film.

the calculated m_{orb}/m_{spin} ratio is $0.06/2.45 \cong 0.024$, which is lower than that of the experimental value of 0.10. The underestimation of m_{orb} is attributed to the underestimated orbital polarization in the framework of a local density approximation.[30] Figures 3(a) and 3(b) exhibit the p-DOSs of N 2*p*, and Figs. 3(c)–3(h) show those of Fe 3*d* orbitals for each Fe site. Here, we pay attention to the four peaks at −8 eV (*a*), −6 eV (*b*), −0.5 eV (*c*), and 3 eV(*d*) in Fig. 3(a). In the p-DOSs of Fe 3*d* orbital at II sites in Figs. 3(c) and 3(e), we can see the peak structures at the same energies as peaks *a*-*d* in Fig. 3(a). In contrast, there are no peaks at those energies in the p-DOSs of Fe 3*d* orbital at I sites in Fig. 3(g), where Fe atoms are separated from the N atom. This indicates that peaks *a*-*d* correspond to the states caused by the band hybridization between the orbitals of Fe 3*d* at II sites and N 2*p*. We find that these peaks *a*-*d* are electronic states generated by σ, π bondings, and π^*, σ^* anti-bondings, respectively, between these orbitals. The σ (σ^*) bonding (anti-bonding) is formed by Fe $3d_{z^2-r^2}$ and N $2p_z$ orbitals, and the π (π^*) bonding (anti-bonding) by Fe $3d_{yz}$, Fe $3d_{zx}$, and N $2p_z$ orbitals. There are electronic states at approximately 3 eV above E_F in the p-DOSs, denoted by arrows in Figs. 3(c) and 3(e), formed by the σ^* anti-bonding. On the other hand, there is no electronic state at this energy in the p-DOSs of Fe 3*d* orbital at I sites in Fig. 3(g). We can also apply the same explanations to the minority spin's p-DOSs in Figs. 3(b), 3(d), 3(f), and 3(h).

Next, we calculated the XAS and XMCD spectra at Fe $L_{2,3}$ and N *K*-edges of Fe_4N by applying these calculated p-DOSs of Fe_4N into Fermi's golden rule. Figures 4(a)–4(d) display the calculated total XAS, partial XAS, total XMCD, and partial XMCD spectra, respectively. In Figs. 4(b) and 4(d), red, green, and blue lines correspond to the spectra calculated from the p-DOSs of Fe atoms located at I, IIA, and IIB sites, respectively. The horizontal axis (photon energy) of the calculated spectra (Fig. 4) is different from that of the experimental ones (Fig. 2), which is mostly due to an incapability of reproducing accurate binding energy of Fe 2*p* orbital as an initial state of the electric dipole transition. We notice that the calculated total XAS and XMCD spectra shown in Figs. 4(a) and 4(c) well explain the line shapes of the experimental results shown in Figs. 2(a) and 2(b), respectively. In particular, the shoulders observed above the main peak structures are theoretically reproduced. In contrast, these shoulders are missing for Fe atoms at I sites [red line in Fig. 4(b)]. Since the Fe atoms at I sites are farther from the N atom than those at II sites, their localized feature should be pronounced. On the other hand, we can clearly see the shoulders in the

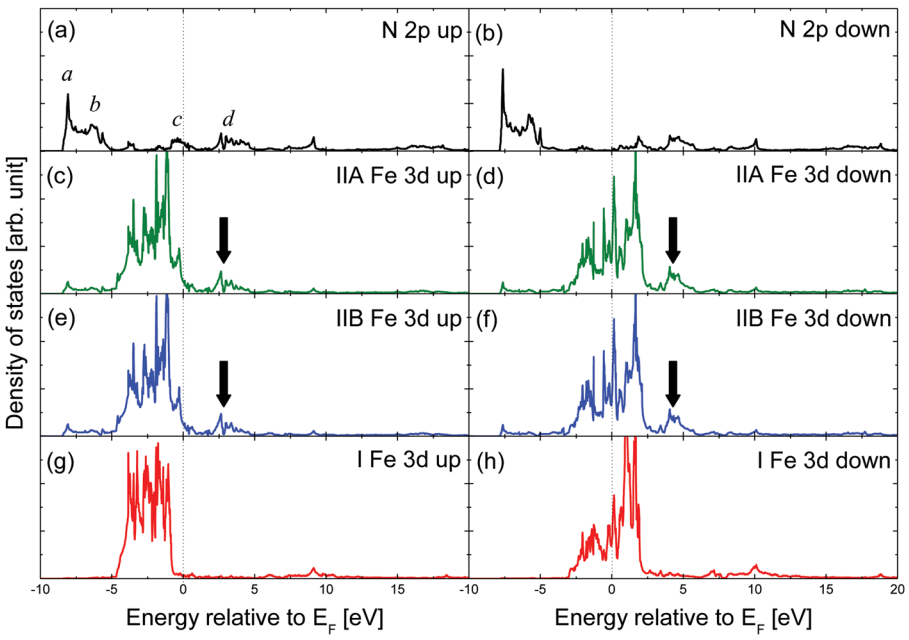

FIG. 3. Calculated projected DOSs on Fe 3*d* and N 2*p* states of the majority and minority spins in Fe_4N when the magnetization points to the [001] direction.

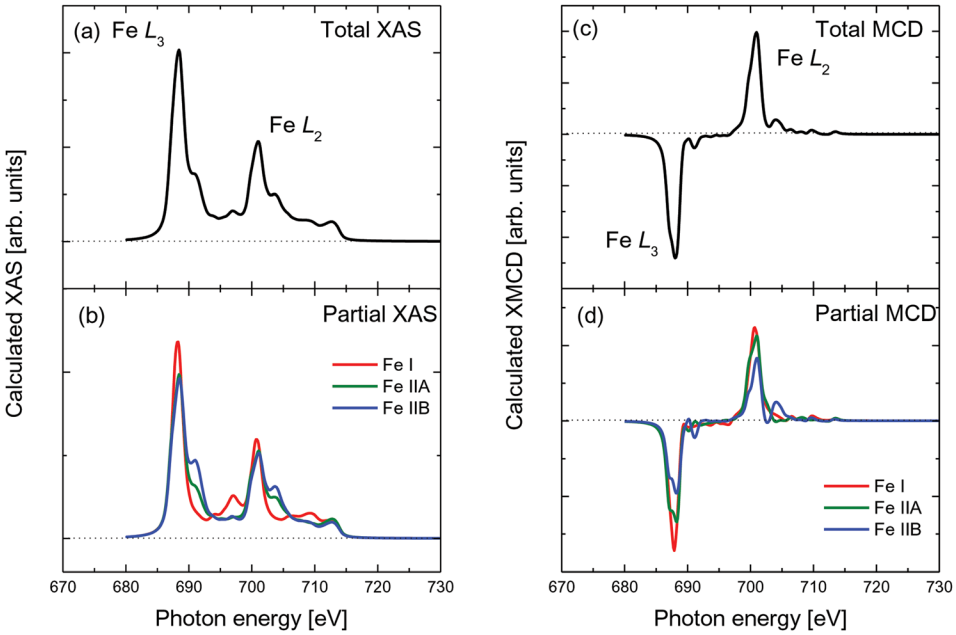

FIG. 4. Calculated (a) total XAS, (b) partial XAS, (c) total XMCD, and (d) partial XMCD spectra at Fe $L_{2,3}$-edges of Fe_4N. The magnetization is assumed to be along the [001] direction.

simulated partial XAS spectra of Fe atoms at II sites [green and blue lines in Fig. 4(b)]. These shoulders are attributed to the dipole transition from the Fe 2*p* core-level to the state generated by the band hybridization between the orbitals of Fe 3*d* at II sites and N 2*p* shown by arrows in the p-DOSs of Figs. 3(c)–3(f). Thus, we conclude that the shoulders shown in Fig. 2(a) reflect the local electronic states of Fe atoms located at II sites. These shoulders were also observed in the XAS spectra at Fe $L_{2,3}$-edges of Fe_4N epitaxial films on Cu(001) substrates measured by *in situ* XMCD measurements,[23] and thereby they are due to intrinsic electronic structures of Fe_4N. We performed the calculation on Co_4N in the same way as that for Fe_4N, and found that the shoulders appeared in the XAS spectrum at Co $L_{2,3}$-edges in Co_4N by the same mechanism as in Fe_4N. We experimentally observed the shoulders in the XAS spectra at Co $L_{2,3}$-edges of Co_4N films[31,32] as well as at Fe and Co $L_{2,3}$-edges of Co_3FeN films.[25,32] We think that these local electronic structures are characteristic of anti-perovskite type ferromagnetic nitrides such as Fe_4N, Co_4N, and their alloys. As to Co_3FeN films, the shoulders were observed at both Fe and Co $L_{2,3}$-edges, meaning that both Fe and Co atoms are located at II sites in the Co_3FeN lattice.[25,32] This speculation about Co-Fe disorder in the Co_3FeN film is consistent with the site-averaged m_{spin} values of Fe and Co atoms in the Co_3FeN film deduced from the measured XMCD spectra.[25,32] This trend is also theoretically supported by the first-principles calculation showing that Co atoms tend to occupy both the I and II sites in $Co_xFe_{4-x}N$ from the viewpoint of total energy.[33] The small shoulders are observed at Fe $L_{2,3}$-edges in the XMCD spectrum shown in Fig. 2(b) denoted by arrows. These smaller shoulders than the main peaks are also theoretically reproduced as shown in Fig. 4(c). In Fig. 4(c), the calculated absolute XMCD intensity at Fe L_3-edge is almost the same as that at Fe L_2-edge, which is inconsistent with the experimental XMCD spectrum in Fig. 2(b). This is attributed to the underestimation of m_{orb} in the first-principles calculation as mentioned above.[30] By applying the sum rule[21,22] into the calculated XMCD spectrum in Fig. 4(c), the m_{orb}/m_{spin} ratio was deduced to be 0.027, which is in good agreement with $m_{orb}/m_{spin} = 0.024$ deduced from the first-principles calculation results shown in Fig. 3. We now confirm that the underestimation of m_{orb} is apparently linked to the strong L_2 XMCD amplitude in Fig. 4(c). We note, however, that the spectral line shapes based on E1 transition are hardly affected by the underestimation.

Next, we move on to the N *K*-edge XAS and XMCD spectra as depicted in Figs. 5(a) and 5(b), respectively, for the Fe_4N layer in sample B. There are four-peak structures around the main peak at photon energies of 398.0 eV (α), 398.5 eV (β), 400.0 eV (γ), and 401.1 eV (δ) in Fig. 5(a). As one can see in Fig. 5(b), the distinct XMCD spectrum is observed with the same sign as XMCD signal of Fe L_3-edge, showing that the N 2*p* orbital of Fe_4N is spin-polarized. In Fig. 5(b), the sign of XMCD signal is slightly negative around 397.5 eV, and it became positive near 398.3 eV. Clear negative XMCD signals are observed around peak β. The XMCD signal is still negative around peak γ, but it becomes positive again near peak δ. Figures 6(a) and 6(b) display the calculated XAS and XMCD spectra, respectively, at N *K*-edges of Fe_4N. We can see the three peak structures labelled as peaks A-C, in Fig. 6(a). The origin of peak A is explained by the dipole transition from the N 1*s* core-level to the hybridization states generated by π^* anti-bonding, and peaks B and C are explained by σ^* anti-bonding between the orbitals of Fe 3*d* at II sites and N 2*p*. Judging from the sign of XMCD signal, correspondence relationship between observed and calculated peaks is α-A, β-B, and δ-C. We are able to simulate well the line shape of XAS and XMCD spectra at N *K*-edge of Fe_4N, especially the variation of the sign of XMCD signal around the main peak structure, although peak γ is not reproduced by the calculation, and the XMCD intensity at peak δ is smaller than that at peak C. Having considered the fact that it is difficult to simulate the

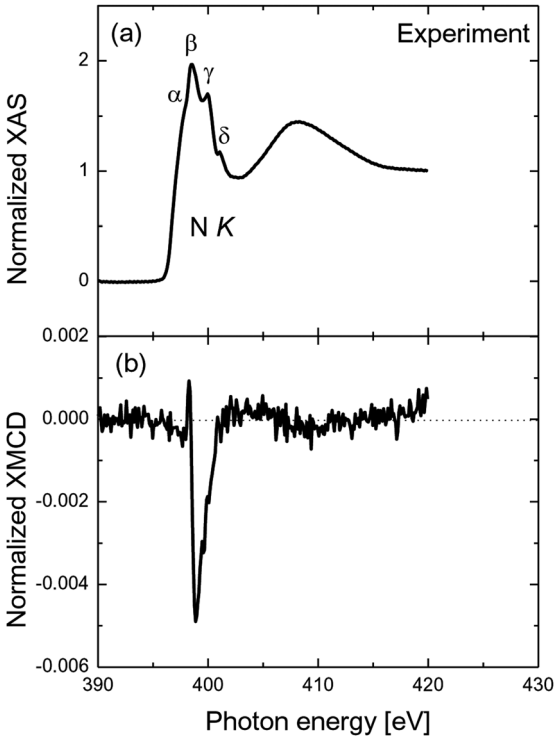

FIG. 5. Experimentally obtained (a) XAS and (b) XMCD spectra at N *K*-edge of the Fe_4N film.

accurate line shape of XAS and XMCD signals above the energy of the N *K*-edge main peak and the effect of N 1*s* core-hole that might sharpen the lowest energy peak that is ignored in the calculation,[34] it is safe to state that we are able to explain the local electronic structure of Fe_4N by comparison of measured XAS and XMCD spectra with those calculated based on the first-principles and Fermi's golden rule. Kokado *et al*. reported that the transfer integral between the Fe 3*d* and N 2*sp* orbitals is small, and the hybridization between these orbitals is weak.[11] However, our experimental results indicate that the band hybridization between the Fe 3*d* and N 2*p* orbitals has a lot of influence on the electronic structure of Fe_4N. The hysteresis loop of the *H* dependence of XMCD intensity measured at N *K*-edge scales with that at Fe L_3-edge.[24] This might be a strong evidence of the band hybridization between the Fe 3*d* and N 2*p* orbitals. We speculate that the Fe 3*d*-N 2*p* band hybridization was formed by Fe 4*sp* orbitals acting as an intermediary between them because the Fe 4*sp* orbitals have a large transfer integral with N 2*sp* and Fe 3*d* orbitals.[11]

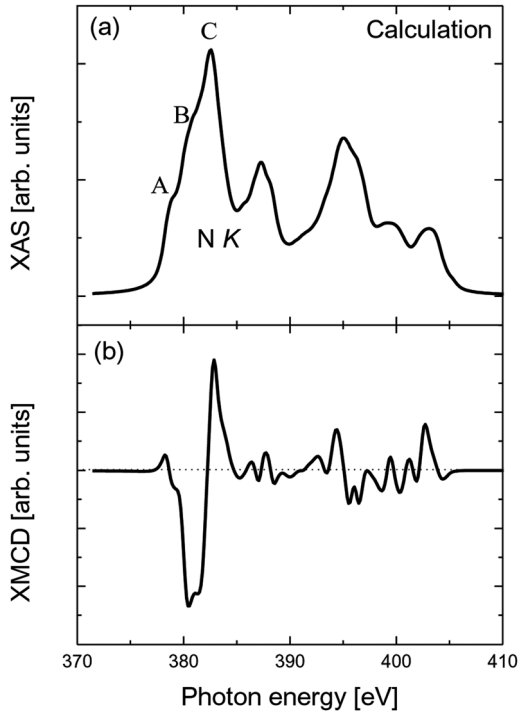

FIG. 6. Calculated (a) XAS and (b) XMCD spectra at N *K*-edge of Fe_4N.

V. CONCLUSION

We measured the XAS and XMCD spectra at Fe $L_{2,3}$ and N *K*-edges of MBE-grown Fe_4N epitaxial films, and compared their line shapes with those calculated. We found that the origin of the shoulders observed at Fe $L_{2,3}$-edges was due to the dipole transition from the Fe 2*p* core-level to the hybridization states formed by σ^* anti-bonding between the orbitals of Fe 3*d* at II sites and N 2*p*. This means that the shoulders reflect the local electronic structure of Fe atoms at II sites. They were also experimentally observed in Co_4N and Co_3FeN films, and thereby we consider that they are the distinctive feature of $Co_xFe_{4-x}N$. The main peak structures of the XAS and XMCD spectra at N *K*-edge were well explained by the dipole transition from the N 1*s* core level to the hybridization states formed by π^* and σ^* anti-bondings between the orbitals of Fe 3*d* at II sites and N 2*p*. We concluded that the band hybridization between these orbitals plays a critical role in defining the electronic structures and physical properties of Fe_4N.

ACKNOWLEDGMENTS

K.I. was financially supported in part by a Grant-in-Aid for JSPS Fellows. The XAS and XMCD measurements were performed at SPring-8 BL23SU under Nanonet Support Proposals (Proposal Nos. 2010A3877 and 2010B3876).

[1]G. Shirane, W. J. Takei, and S. L. Ruby, Phys. Rev. **126**, 49 (1962).
[2]W. J. Takei, R. R. Heikes, and G. Shirane, Phys. Rev. **125**, 1893 (1962).
[3]D. Fruchart, D. Givord, P. Convert, P. Heritier, and J. P. Senateur, J. Phys. F: Met. Phys. **9**, 2431 (1979).
[4]J. M. D. Coey and P. A. I. Smith, J. Magn. Magn. Mater. **200**, 405 (1999).
[5]E. L. P. Blanca, J. Desimoni, N. E. Christensen, H. Emmerich, and S. Cottenier, Phys. Status Solidi B **246**, 909 (2009).
[6]D. M. Borsa, S. Grachev, D. O. Boerma, and J. W. J. Kerssemakers, Appl. Phys. Lett. **79**, 994 (2001).
[7]K. R. Nikolaev, I. N. Krivorotov, E. D. Dahlberg, V. A. Vas'ko, S. Urazhdin, R. Loloee, and W. P. Pratt, Jr., Appl. Phys. Lett. **82**, 4534 (2003).
[8]J. M. Gallego, S. Y. Grachev, D. M. Borsa, D. O. Boerma, D. Écija, and R. Miranda, Phys. Rev. B **70**, 115417 (2004).
[9]S. Atiq, H. S. Ko, S. A. Siddiqi, and S. C. Shin, Appl. Phys. Lett. **92**, 222507 (2008).
[10]K. Ito, G. H. Lee, H. Akinaga, and T. Suemasu, J. Cryst. Growth **322**, 63 (2011).
[11]S. Kokado, N. Fujima, K. Harigaya, H. Shimizu, and A. Sakuma, Phys. Rev. B **73**, 172410 (2006).

[12]A. Narahara, K. Ito, T. Suemasu, Y. K. Takahashi, A. Rajanikanth, and K. Hono, Appl. Phys. Lett. **94**, 202502 (2009).
[13]K. Ito, K. Okamoto, K. Harada, T. Sanai, K. Toko, S. Ueda, Y. Imai, T. Okuda, K. Miyamoto, A. Kimura, and T. Suemasu, J. Appl. Phys. **112**, 013911 (2012).
[14]M. Tsunoda, Y. Komasaki, S. Kokado, S. Isogami, C. C. Chen, and M. Takahashi, Appl. Phys. Express **2**, 083001 (2009).
[15]M. Tsunoda, H. Takahashi, S. Kokado, Y. Komasaki, A. Sakuma, and M. Takahashi, Appl. Phys. Express **3**, 113003 (2010).
[16]K. Ito, K. Kabara, H. Takahashi, T. Sanai, K. Toko, T. Suemasu, and M. Tsunoda, Jpn. J. Appl. Phys. **51**, 068001 (2012).
[17]S. Kokado, M. Tsunoda, K. Harigaya, and A. Sakuma, J. Phys. Soc. Jpn. **81**, 024705 (2012).
[18]Y. Komasaki, M. Tsunoda, S. Isogami, and M. Takahashi, J. Appl. Phys. **105**, 07C928 (2009).
[19]S. Isogami, M. Tsunoda, Y. Komasaki, A. Sakuma, and M. Takahashi, Appl. Phys. Express **3**, 103002 (2010).
[20]S. Isogami, M. Tsunoda, M. Oogane, A. Sakuma, and M. Takahashi, Appl. Phys. Express **6**, 063004 (2013).
[21]B. T. Thole, P. Carra, F. Sette, and G. van der Laan, Phys. Rev. Lett. **68**, 1943 (1992).
[22]P. Carra, B. T. Thole, M. Altarelli, and X. D. Wang, Phys. Rev. Lett. **70**, 694 (1993).
[23]Y. Takagi, K. Isami, I. Yamamoto, T. Nakagawa, and T. Yokoyama, Phys. Rev. B **81**, 035422 (2010).
[24]K. Ito, G. H. Lee, K. Harada, M. Suzuno, T. Suemasu, Y. Takeda, Y. Saitoh, M. Ye, A. Kimura, and H. Akinaga, Appl. Phys. Lett. **98**, 102507 (2011).
[25]K. Ito, T. Sanai, Y. Yasutomi, S. Zhu, K. Toko, Y. Takeda, Y. Saitoh, A. Kimura, and T. Suemasu, J. Appl. Phys. **115**, 17C712 (2014).
[26]I. A. Kowalik, A. Persson, M. A. Nino, A. Navarro-Quezada, B. Faina, A. Bonanni, T. Dietl, and D. Arvanitis, Phys. Rev. B **85**, 184411 (2012).
[27]Y. Saitoh, Y. Fukuda, Y. Takeda, H. Yamagami, S. Takahashi, Y. Asano, T. Hara, K. Shirasawa, M. Takeuchi, T. Tanaka, and H. Kitamura, J. Synchrotron Radiat. **19**, 388 (2012).
[28]T. Ueda, M. Kodera, K. Yamauchi, and T. Oguchi, J. Phys. Soc. Jpn. **82**, 094718 (2013), and references therein.
[29]M. Kallmayer, P. Klaer, H. Schneider, G. Jakob, H. J. Elmers, D. Legut, and P. M. Oppeneer, Phys. Rev. B **84**, 054448 (2011).
[30]P. Söderlind, O. Eriksson, B. Johansson, R. C. Albers, and A. M. Boring, Phys. Rev. B **45**, 12911 (1992).
[31]K. Ito, K. Harada, K. Toko, M. Ye, A. Kimura, Y. Takeda, Y. Saitoh, H. Akinaga, and T. Suemasu, Appl. Phys. Lett. **99**, 252501 (2011).
[32]K. Ito, T. Sanai, S. Zhu, Y. Yasutomi, K. Toko, S. Honda, S. Ueda, Y. Takeda, Y. Saitoh, Y. Imai, A. Kimura, and T. Suemasu, Appl. Phys. Lett. **103**, 232403 (2013).
[33]P. Monachesi, T. Björkman, T. Gasche, and O. Eriksson, Phys. Rev. B **88**, 054420 (2013).
[34]V. N. Strocov, T. Schmitt, J.-E. Rubensson, P. Blaha, T. Paskova, and P. O. Nilsson, Phys. Rev. B **72**, 085221 (2005).